

Article

Analysis of Entropy Generation in Mixed Convective Peristaltic Flow of Nanofluid

Tasawar Hayat ^{1,2}, Sadaf Nawaz ^{1,*}, Ahmed Alsaedi ² and Maimona Rafiq ¹

¹ Department of Mathematics, Quaid-I-Azam University, Islamabad 45320, Pakistan; fmgpak@gmail.com (T.H.); maimona88@gmail.com (M.R.)

² Nonlinear and Applied Mathematics (NAAM) Research Group, Department of Mathematics, King Abdulaziz University, Jeddah 21589, Saudi Arabia; aalsaedi@kau.edu.sa

* Correspondence: sadafnawaz26@gmail.com; Tel.: +92-51-9064-2172

Academic Editor: Brian Agnew

Received: 28 June 2016; Accepted: 23 September 2016; Published: 30 September 2016

Abstract: This article examines entropy generation in the peristaltic transport of nanofluid in a channel with flexible walls. Single walled carbon nanotubes (SWCNT) and multiple walled carbon nanotubes (MWCNT) with water as base fluid are utilized in this study. Mixed convection is also considered in the present analysis. Viscous dissipation effect is present. Moreover, slip conditions are encountered for both velocity and temperature at the boundaries. Analysis is prepared in the presence of long wavelength and small Reynolds number assumptions. Two phase model for nanofluids are employed. Nonlinear system of equations for small Grashof number is solved. Velocity and temperature are examined for different parameters via graphs. Streamlines are also constructed to analyze the trapping. Results show that axial velocity and temperature of the nanofluid decrease when we enhance the nanoparticle volume fraction. Moreover, the wall elastance parameter shows increase in axial velocity and temperature, whereas decrease in both quantities is noticed for damping coefficient. Decrease is notified in Entropy generation and Bejan number for increasing values of nanoparticle volume fraction.

Keywords: Velocity and thermal slip conditions; peristalsis; water; compliant walls; carbon nanotubes; mixed convection; entropy generation

1. Introduction

Due to ample applications the nanofluids have gained a lot of interest among researchers. The nanofluids consist of particles of nanosize in the base fluid. Base fluids usually utilized for this purpose are kerosene oil, water, ethylene-glycol, etc. The nanoparticles used in the nanofluids are of different types including the metals, metallic oxides, oxides, carbides, carbon nanotubes, etc. The characteristics of the nanofluids highly depend upon the shape, size and material of the nanoparticles. The nanoparticles are efficient for the enhancement of thermal conductivity. Moreover, the shape of the nanoparticles is important. The cylindrical shape nanoparticles are more effective for transfer of heat than the spherical shape. Keeping all these facts in mind, researchers in this field are engaged in different experimental and theoretical works to utilize nanofluids in different applications. Some of these results can be seen through the applications of nanofluids in automobiles as coolant, microelectronics, microchips in computers, food processing, fuel cells, transportation, biomedicine, solid state lightening and manufacturing, etc. The word nanofluid was first coined by Choi [1]. Afterwards, different researchers worked in this field under different aspects. Different models of the effective thermal conductivity, such as Maxwell, Hamilton-Crosser, etc., were used for different types of nanoparticles. One of the models of effective thermal conductivity related to the nanofluids is Xue [2] model. The Xue model is utilized for the cases of single walled

carbon nanotubes (SWCNT) and multiple walled carbon nanotubes (MWCNT), as these nanoparticles have large axial ratio, whereas the previous models of effective thermal conductivity are best suited for the nanoparticles with small axial ratios. Xue proposed a model based on Maxwell theory. This model also describes the properties of space distribution of the carbon nanotubes (CNTs) on thermal conductivity. Some literature shedding light on the flows nanofluids can be seen through the References [3–13].

The peristalsis is also an interesting topic attaining the fame day by day. Basically peristaltic mechanism consists of contraction and expansion activities, which propel the material forward. This process has many industrial and biomedical applications. Peristalsis is found extensively in many physiological systems like the transportation of urine from kidney to bladder, lymph transport in the lymphatic vessels, transport of bile in bile duct, spermatic flow in the male reproductive tract, etc. In biomedical applications, peristalsis is utilized in dialysis machine, open heart bypass machine, etc. One of the advantages of peristalsis is that it prevents the direct contact of the fluid with the machinery to avoid contamination. This process is also applied in the transport of sanitary fluid and for corrosive and sensitive fluids transport. Latham [14] was the first who initially investigated the motion of fluid in peristaltic pump. He discussed the characteristics of pressure rise versus flow rate. Shapiro [15] aimed to study peristaltic wave as a pump. He adopted long wavelength and low Reynolds number assumptions to consider the flow inertia-free. Weinberg [16] studied the peristaltic phenomenon with reference to ureter functioning. Srinivas and Kothandapani [17] discussed the peristaltic transport of viscous fluid in an asymmetric channel. Peristaltic motion of viscous fluid with temperature dependent viscosity is analyzed by Asghar et al. [18]. Peristaltic phenomenon through eccentric cylinders is observed by Mekheimer et al. [19]. Hayat et al. [20] explained the rotating effect in peristaltic transport of Jeffrey fluid. Peristalsis of second order fluid is investigated by Elmaboud et al. [21]. Main findings of the studies [17–21] showed that amplitude of temperature reduces for increasing phase difference and radiation parameter. Ramesh [22] explained the effects of heat and mass transfer in peristaltic flow of couple stress fluid by considering inclined magnetohydrodynamic (MHD) effects. Abd-Alla et al. [23] examined peristalsis of Jeffrey fluid in a tube. Investigation of peristalsis with MHD and slip conditions is made by Sinha et al. [24]. Analysis of peristaltic transport of dusty fluid with chemical reaction is presented by Muthuraj et al. [25]. Peristaltic motion of second grade fluid in a tube is examined by Hameed et al. [26]. Peristaltic motion of Jeffrey fluid in presence of MHD and slip conditions is investigated by Ellahi et al. [27]. Results obtained through refs. [22–27] showed that the magnetic field greatly affects the velocity and temperature of different non-Newtonian fluids. Behaviors of velocity and temperature are found to be of decrease. Consideration for peristaltic motion of nanofluids is made by Abbasi et al. [28–30]. Furthermore, Shehzad et al. [31] and Hayat et al. [32–34] studied the peristaltic motion of nanofluids subject to slip condition, Joule heating and Soret and Dufour effects. Impact of Hall effect on interaction of pulsatile and peristaltic induced flows of a particle-fluid suspension is analyzed by Gad et al. [35]. In these studies, we have noticed that Brownian motion parameter shows similar behavior on velocity and temperature while thermophoretic parameter shows opposite influence. Moreover heat transfer rate enhances with the use of nanofluid.

Entropy is often considered as a measure of disorder or a measure of progress towards thermodynamic equilibrium. It is also defined as the measure of the number of specific ways in which a thermodynamic system may be arranged. Due to occurrence of irreversible processes the entropy of system gets changed. These changes may occur in the form such as heat flow through a thermal resistance, unrestrained chemical reaction, Joule heating, friction between solid surfaces, fluid viscosity and turbulence within a system. Literature is scarce on the peristalsis with entropy generation. Only few researches have been yet made in this direction (see References [36–38]). The purpose here is to venture further in this regime. Thus, entropy generation effect in peristalsis through carbon nanotubes is explored here. Mixed convection is also taken in this problem. SWCNT and MWCNT with water as based fluid are considered in this analysis. Slip boundary conditions are employed for this study. Analysis is done in view of lubrication approach. Equations for small Grashof number are

solved. The graphs for axial velocity and temperature are plotted against for parameters of interest. Streamlines are plotted for the sake of trapping. Moreover, the graphs of entropy generation and entropy generation numbers versus different pertinent parameters are also plotted and studied.

2. Flow Modeling

We examined the mixed convective peristaltic transport of an incompressible nanofluid in a channel of width $2d$. The channel walls are taken as flexible. Two types of nanofluids namely, SWCNT–water nanofluid and MWCNT–water nanofluid are considered in this analysis. The walls are placed at the position $y = \pm\eta$ where + and – denote the right and left walls, respectively. Both walls are maintained at constant temperature T_0 . The sinusoidal waves propagate along the length of the channel which set the fluid in motion. The waves move with constant speed c , have wavelength λ and amplitude b . Walls geometry (Figure 1) is given by:

$$y = \pm\eta(x, t) = \pm \left[d + b \sin \frac{2\pi}{\lambda} (x - ct) \right], \quad (1)$$

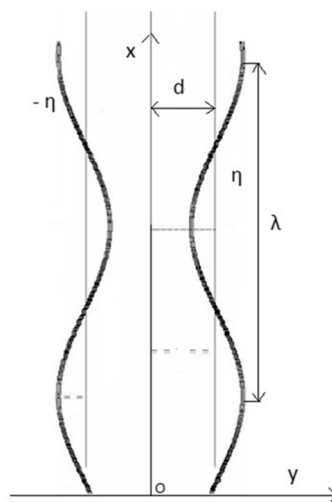


Figure 1. Flow Geometry.

The governing equations for the considered flow analysis are:

$$\frac{\partial u}{\partial x} + \frac{\partial v}{\partial y} = 0, \quad (2)$$

$$\rho_{eff} \left(\frac{\partial}{\partial t} + u \frac{\partial}{\partial x} + v \frac{\partial}{\partial y} \right) u = - \frac{\partial p}{\partial x} + \mu_{eff} \left[\frac{\partial^2 u}{\partial x^2} + \frac{\partial^2 u}{\partial y^2} \right] + g(\rho\beta)_{eff} (T - T_0), \quad (3)$$

$$\rho_{eff} \left(\frac{\partial}{\partial t} + u \frac{\partial}{\partial x} + v \frac{\partial}{\partial y} \right) v = - \frac{\partial p}{\partial y} + \mu_{eff} \left[\frac{\partial^2 v}{\partial x^2} + \frac{\partial^2 v}{\partial y^2} \right], \quad (4)$$

$$(\rho C)_{eff} \left(\frac{\partial}{\partial t} + u \frac{\partial}{\partial x} + v \frac{\partial}{\partial y} \right) T = K_{eff} \left[\frac{\partial^2 T}{\partial x^2} + \frac{\partial^2 T}{\partial y^2} \right] + \mu_{eff} \left[2 \left(\left(\frac{\partial u}{\partial x} \right)^2 + \left(\frac{\partial v}{\partial y} \right)^2 \right) + \left(\frac{\partial u}{\partial y} + \frac{\partial v}{\partial x} \right)^2 \right]. \quad (5)$$

In above equations, p is the pressure, μ_{eff} is the effective viscosity, g is the acceleration due to gravity, ρ_{eff} is the effective density, K_{eff} is the effective thermal conductivity, and $(\rho C)_{eff}$ and $(\rho\beta)_{eff}$ are the effective heat capacity and the effective thermal expansion of the nanofluid, respectively. Moreover, u and v define the velocity components in the x and y directions, respectively.

Quantities in two phase model are given as [39–41]:

$$\begin{aligned} \rho_{eff} &= (1 - \varphi)\rho_f + \varphi\rho_p, (\rho C)_{eff} = (1 - \varphi)(\rho C)_f + \varphi(\rho C)_p, \\ (\rho\beta)_{eff} &= (1 - \varphi)\rho_f\beta_f + \varphi\rho_p\beta_p, \mu_{eff} = \mu_f\left(1 - \frac{\varphi_a}{\varphi_m}\right)^{-2}, \\ \frac{K_{eff}}{K_f} &= \frac{(1 - \varphi) + 2\varphi\frac{K_{CNT}}{K_f}\ln\frac{K_{CNT}+K_f}{2K_f}}{(1 - \varphi) + 2\varphi\frac{K_f}{K_{CNT}-K_f}\ln\frac{K_{CNT}+K_f}{2K_f}}. \end{aligned} \tag{6}$$

The quantities ρ , C and β elucidate the respective density, the specific heat and the thermal expansion coefficients, respectively, whereas subscripts p and f symbolize nanoparticle and fluid, respectively. Here, φ represents the volume fraction of nanoparticles used to prepare nanofluids. The viscosity model given in Equation (6) is modified Maron–Pierce model. Here, φ_m is the maximum packing volume fraction, whereas φ_a is the effective volume fraction of aggregates given by:

$$\varphi_a = \varphi \left(\frac{a_a}{a}\right)^{3-D},$$

where a_a is the effective radii of aggregates, a is radius of nanoparticles and D is fractal index. The fractal index D can depend on the type of aggregation, particle size and shape and shear flow condition. For aggregating nanofluids with nanorods or nanotubes, D varies between 1.5 and 2.45.

The previous models (Maxwell, Hamilton–Crosser, etc.) are used only for spherical or rotational elliptical particles with small axial ratio. Xue [2] proposed a theoretical model based on Maxwell theory considering rotational elliptical nanotubes with very large axial ratio. It also describes the properties of space distribution of the CNTs on thermal conductivity.

Numerical values of the thermophysical parameters of base fluid and nanoparticles are mentioned in Table 1.

Table 1. Thermophysical parameters of water and nanoparticles [42,43].

	ρ (kg·m ⁻³)	C_p (J·kg ⁻¹ ·K ⁻¹)	K (W·m ⁻¹ ·K ⁻¹)	β (1/K) × 10 ⁻⁶
H₂O	997.1	4179	0.613	210
SWCNT	2600	425	6600	19
MWCNT	1600	796	3000	21

The conditions are

$$u \pm \beta_1 S_{xy} = 0, \text{ at } y = \pm\eta, \tag{7}$$

$$\left[-\tau\frac{\partial^3}{\partial x^3} + m\frac{\partial^3}{\partial x\partial t^2} + d_1\frac{\partial^2}{\partial t\partial x}\right]\eta = \frac{\partial S_{xy}}{\partial y} + \frac{\partial S_{xx}}{\partial x} - \rho_f\left[\frac{\partial u}{\partial t} + u\frac{\partial u}{\partial x} + v\frac{\partial u}{\partial y}\right] + g(\rho\beta)_{eff}(T - T_0), \text{ at } y = \pm\eta, \tag{8}$$

$$T \pm \gamma_1\frac{\partial T}{\partial y} = T_0, \text{ at } y = \pm\eta. \tag{9}$$

The dimensionless quantities are introduced as:

$$\begin{aligned} x^* &= \frac{x}{\lambda}, y^* = \frac{y}{d}, u^* = \frac{u}{c}, v^* = \frac{v}{c}, t^* = \frac{ct}{\lambda}, \eta^* = \frac{\eta}{d}, \\ p^* &= \frac{d^2 p}{c\lambda\mu_f}, Re = \frac{\rho_f cd}{\mu_f}, \theta = \frac{T - T_0}{T_0}, Pr = \frac{\mu_f C_f}{K_f}, \\ Ec &= \frac{c^2}{C_f T_0}, Br = PrEc, Gr = \frac{g\rho_f\beta_f T_0 d^2}{c\mu_f}, \\ u &= \frac{\partial\psi}{\partial y}, v = -\delta\frac{\partial\psi}{\partial x}. \end{aligned} \tag{10}$$

where Re , Pr , Ec , Br and Gr represent the Reynolds, Prandtl, Eckert, Brinkman and Grashof numbers, respectively.

By large wavelength and small Reynolds number one obtains

$$\frac{\partial p}{\partial x} = \left(1 - \frac{\varphi_a}{\varphi_m}\right)^{-2} \frac{\partial^3 \psi}{\partial y^3} + Gr A_2 \theta, \quad (11)$$

$$\frac{\partial p}{\partial y} = 0, \quad (12)$$

$$A_3 \frac{\partial^2 \theta}{\partial y^2} + Br \left(1 - \frac{\varphi_a}{\varphi_m}\right)^{-2} \left(\frac{\partial^2 \psi}{\partial y^2}\right)^2 = 0, \quad (13)$$

$$A_2 = 1 - \varphi + \varphi \left(\frac{(\rho\beta)_p}{(\rho\beta)_f}\right), \quad (14)$$

$$A_3 = \frac{(1 - \varphi) + 2\varphi \frac{K_{CNT}}{K_{CNT} - K_f} \ln \frac{K_{CNT} + K_f}{2K_f}}{(1 - \varphi) + 2\varphi \frac{K_f}{K_{CNT} - K_f} \ln \frac{K_{CNT} + K_f}{2K_f}}.$$

The dimensionless form of boundary conditions is:

$$\frac{\partial \psi}{\partial y} \pm \beta \frac{\partial^2 \psi}{\partial y^2} = 0, \theta \pm \gamma \frac{\partial \theta}{\partial y} = 0, \text{ at } y = \pm \eta, \quad (15)$$

$$\left[E_1 \frac{\partial^3}{\partial x^3} + E_2 \frac{\partial^3}{\partial x \partial t^2} + E_3 \frac{\partial^2}{\partial t \partial x} \right] \eta = \left(1 - \frac{\varphi_a}{\varphi_m}\right)^{-2} \frac{\partial^3 \psi}{\partial y^3} + Gr A_2 \theta, \text{ at } y = \pm \eta. \quad (16)$$

where β and γ are the dimensionless form of slip parameters for velocity and temperature, respectively.

Entropy Generation and Viscous Dissipation

The viscous dissipation effect in dimensional form can be defined as:

$$\Phi = \mu_{eff} \left[2 \left(\left(\frac{\partial u}{\partial x} \right)^2 + \left(\frac{\partial v}{\partial y} \right)^2 \right) + \left(\frac{\partial u}{\partial y} + \frac{\partial v}{\partial x} \right)^2 \right]. \quad (17)$$

The volumetric entropy generation in dimensional form is given by [40]:

$$S_{gen}''' = \frac{K_{eff}}{\Theta_0^2} \left(\left(\frac{\partial T}{\partial x} \right)^2 + \left(\frac{\partial T}{\partial y} \right)^2 \right) + \frac{\Phi}{\Theta_0}. \quad (18)$$

The entropy generation in dimensionless form become [40]:

$$N_s = \frac{S_{gen}'''}{S_G'''} = A_3 \left(\frac{\partial \theta}{\partial y} \right)^2 + \frac{\Lambda Br}{\left(1 - \frac{\varphi_a}{\varphi_m}\right)^2} \left(\frac{\partial^2 \psi}{\partial y^2} \right)^2, \quad (19)$$

$$S_G''' = \frac{K_f T_0^2}{\Theta_0^2 d^2}, \Lambda = \frac{\Theta_0}{T_0}. \quad (20)$$

Here, Θ_0 elucidates the reference temperature.

Now, we define the Bejan number as:

$$Be = \frac{N_{s_{cond}}}{N_{s_{cond}} + N_{s_{visc}}}. \quad (21)$$

Equation (18) comprises two parts: one part consists of entropy generation because of finite temperature difference (Ns_{cond}), and the other part comprises of entropy generation due to viscous dissipation effects (Ns_{visc}).

3. Solution Methodology

In order to find the solution to the above-mentioned problem, we look for the perturbation method for small Grashof number. The resulting zeroth and first order systems and their solutions are as follows:

3.1. Zeroth Order Systems and Solutions

The stream function and temperature statements at this order are

$$\frac{\partial^4 \psi_0}{\partial y^4} = 0, \quad (22)$$

$$A_3 \frac{\partial^2 \theta_0}{\partial y^2} + Br \left(1 - \frac{\varphi_a}{\varphi_m}\right)^{-2} \left(\frac{\partial^2 \psi_0}{\partial y^2}\right)^2 = 0, \quad (23)$$

$$\frac{\partial \psi_0}{\partial y} \pm \beta \frac{\partial^2 \psi_0}{\partial y^2} = 0, \left[E_1 \frac{\partial^3}{\partial x^3} + E_2 \frac{\partial^3}{\partial x \partial t^2} + E_3 \frac{\partial^2}{\partial t \partial x} \right] \eta = \left(1 - \frac{\varphi_a}{\varphi_m}\right)^{-2} \frac{\partial^3 \psi_0}{\partial y^3}, \text{ at } y = \pm \eta, \quad (24)$$

$$\theta_0 \pm \gamma \frac{\partial \theta_0}{\partial y} = 0, \text{ at } y = \pm \eta. \quad (25)$$

The solutions of stream function and temperature are

$$\psi_0 = C_1 + y(C_2 + y(C_3 + C_4 y)), \quad (26)$$

$$\theta_0 = -\frac{A_1 Br (C_3 + 3C_4 y)^4}{27 A_3 C_4^2} + F_1 + y F_2. \quad (27)$$

3.2. First Order Systems and Solutions

Here one has

$$\left(1 - \frac{\varphi_a}{\varphi_m}\right)^{-2} \frac{\partial^4 \psi_1}{\partial y^4} + A_2 \frac{\partial \theta_0}{\partial y} = 0, \quad (28)$$

$$A_3 \frac{\partial^2 \theta_1}{\partial y^2} + Br \left(1 - \frac{\varphi_a}{\varphi_m}\right)^{-2} \left(2 \frac{\partial^2 \psi_0}{\partial y^2} \frac{\partial^2 \psi_1}{\partial y^2}\right) = 0, \quad (29)$$

$$\frac{\partial \psi_1}{\partial y} \pm \beta \frac{\partial^2 \psi_1}{\partial y^2} = 0, \left(1 - \frac{\varphi_a}{\varphi_m}\right)^{-2} \frac{\partial^3 \psi_1}{\partial y^3} + A_2 \theta_0 = 0 \text{ at } y = \pm \eta, \quad (30)$$

$$\theta_1 \pm \gamma \frac{\partial \theta_1}{\partial y} = 0, \text{ at } y = \pm \eta. \quad (31)$$

The solution expressions are

$$\psi_1 = \frac{A_2 \left(-\frac{9}{8} A_3 C_4^2 F_2 y^4 + \frac{A_1 Br (C_3 + 3C_4 y)^7}{5670 C_4^3} \right)}{27 A_1 A_3 C_4^2} + B_1 + y B_2 + y^2 B_3 + y^3 B_4, \quad (32)$$

$$\theta_1 = -\frac{4A_1B_3BrC_3y^2}{A_3} - \frac{2A_1A_2Br^2C_3^6y^2}{405A_3^2C_4^3} - \frac{4A_1B_4BrC_3y^3}{A_3} - \frac{4A_1A_2Br^2C_3^5y^3}{135A_3^2C_4^2} - \frac{4A_1B_3BrC_4y^3}{A_3} - \frac{A_1A_2Br^2C_3^4y^4}{9A_3^2C_4} - \frac{6A_1B_4BrC_4y^4}{A_3} + \frac{A_2BrC_3F_2y^4}{6A_3} - \frac{4A_1A_2Br^2C_3^3y^5}{15A_3^2} + \frac{3A_2BrC_4F_2y^5}{10A_3} - \frac{2A_1A_2Br^2C_3^2C_4y^6}{5A_3^2} - \frac{12A_1A_2Br^2C_3C_4^2y^7}{35A_3^2} - \frac{9A_1A_2Br^2C_4^3y^8}{70A_3^2} + G_1 + yG_2. \tag{33}$$

where C_i, F_i, B_i and G_i are constants that can be evaluated through MATHEMATICA 9.0.

4. Discussion

Here we analyzed the results through graphs. Figure 2 is plotted to analyze the behavior of nanoparticle volume fraction on the velocity. It is seen that velocity is decreasing function of nanoparticle volume fraction in both cases of SWCNT and MWCNT. The reason behind this fact is that the fluid offered more resistance as the nanoparticle volume fraction increases. Moreover, the velocity for MWCNT is greater than the SWCNT. To illustrate the behavior of slip parameter on the velocity profile we sketched Figure 3. Obviously, the velocity is an increasing function of slip parameter. An increase in slip parameter reduces the friction between the walls and fluid so the velocity profile shows increasing behavior via larger the slip parameter. The velocity profile for the case of MWCNT is larger than for the case of SWCNT. Figure 4 elucidates the impact of Grashof number on the axial velocity profile. The velocity of the nanofluid increases when the Grashof number attains larger values. In fact, viscosity decreases with increasing Gr . This results in increased of velocity. Figure 5 represents the influence of wall parameters on the axial velocity profile. The axial velocity increases in cases of E_1 and E_2 , which are the elastance parameters, whereas it decreases for the case of wall damping parameter E_3 . In fact, an increase in elastance parameters provide flexibility of walls, which causes increase in velocity while damping force provided by wall resists the fluid flow, and, as a result, the velocity decreases. In all cases, the velocity profile for MWCNT is greater than the SWCNT. The results obtained from present study for velocity are found similar qualitatively to the one observed by Akbar et al. [40].

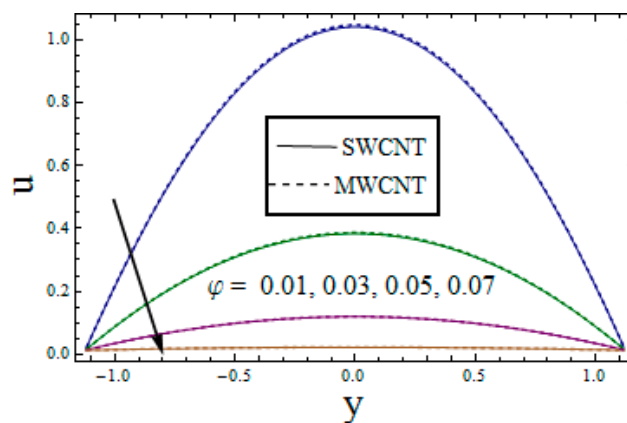


Figure 2. φ versus u when $E_1 = 0.02, E_2 = 0.01, E_3 = 0.01, t = 0.1, x = 0.2, \varepsilon = 0.2, Br = 3.0, Gr = 3.0, \beta = 0.01, \gamma = 0.01$.

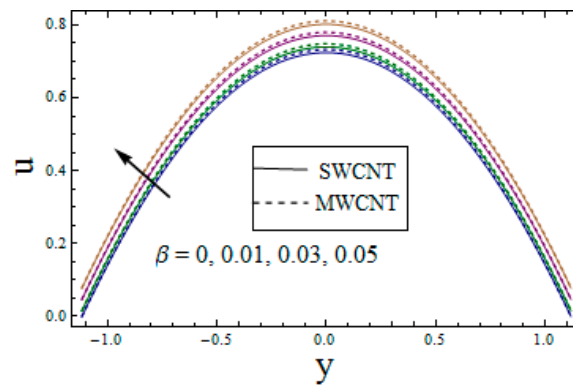


Figure 3. β versus u when $E_1 = 0.02, E_2 = 0.01, E_3 = 0.01, t = 0.1, x = 0.2, \varepsilon = 0.2, Br = 3.0, Gr = 3.0, \varphi = 0.15, \gamma = 0.01$.

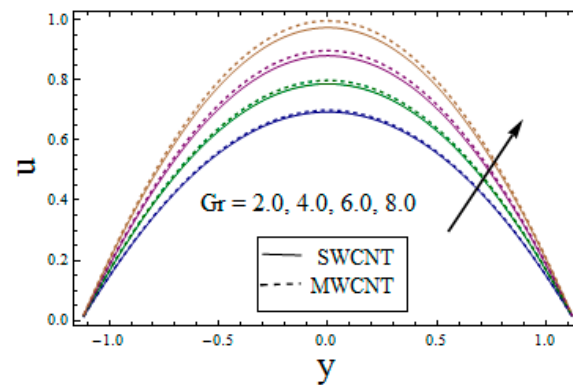


Figure 4. Gr versus u when $E_1 = 0.02, E_2 = 0.01, E_3 = 0.01, t = 0.1, x = 0.2, \varepsilon = 0.2, Br = 3.0, \varphi = 0.15, \beta = 0.01, \gamma = 0.01$.

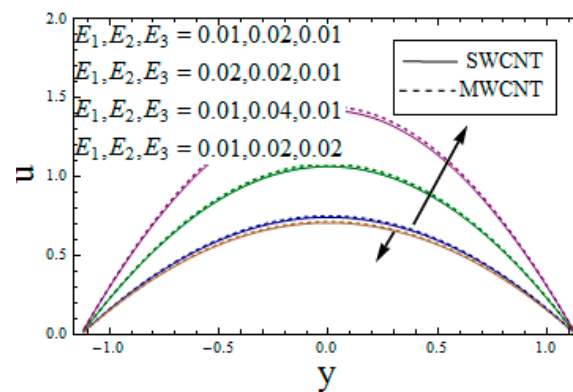


Figure 5. E_1, E_2, E_3 versus u when $\varphi = 0.15, t = 0.1, x = 0.2, \varepsilon = 0.2, Br = 3.0, Gr = 3.0, \beta = 0.01, \gamma = 0.01$.

Figure 6 depicts the influence of nanoparticle volume fraction on the temperature profile. The temperature shows decreasing effect when the nanoparticle volume fraction enlarges. An increase in nanoparticles volume fraction enhances the thermal conductivity of the system. As a result the heat transfer rate decreases which result in decay of temperature. It is also noted that the temperature for MWCNT is greater than SWCNT. Figure 7 explains impact of thermal slip parameter on the temperature profile. Enhancement is observed in temperature as the thermal slip parameter attains large value. As we increase the slip parameter the contact of wall and fluid becomes small.

Hence causing less heat transfer between wall and fluid results in increase of temperature. To know the influence of Grashof number on the temperature profile Figure 8 is sketched. Increment is noted in temperature when Grashof number is increased. Influence of wall parameters on θ is portrayed through Figure 9. Same behavior is noticed in case of temperature when compared with velocity. In all cases, the temperature is larger for MWCNT than SWCNT.

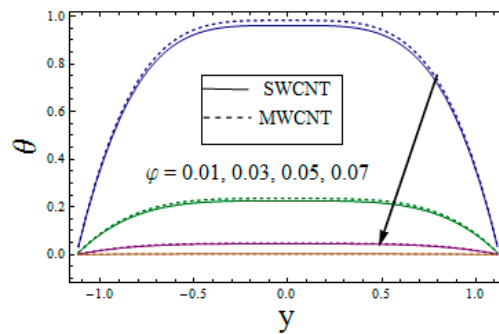


Figure 6. $c\varphi$ versus θ when $E_1 = 0.02, E_2 = 0.01, E_3 = 0.01, t = 0.1, x = 0.2, \varepsilon = 0.2, Br = 3.0, Gr = 3.0, \beta = 0.01, \gamma = 0.01$.

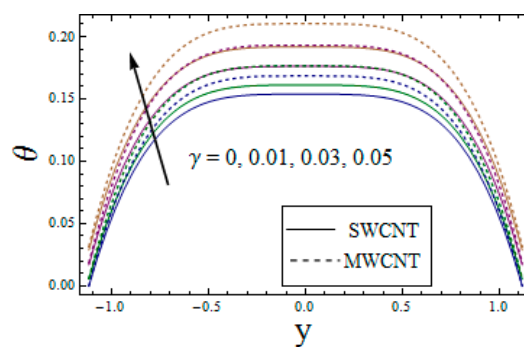


Figure 7. γ versus θ when $E_1 = 0.02, E_2 = 0.01, E_3 = 0.01, t = 0.1, x = 0.2, \varepsilon = 0.2, Br = 3.0, Gr = 3.0, \beta = 0.01, \varphi = 0.15$.

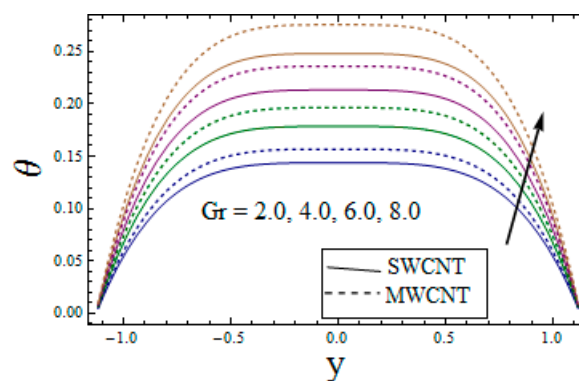


Figure 8. Gr versus θ when $E_1 = 0.02, E_2 = 0.01, E_3 = 0.01, t = 0.1, x = 0.2, \varepsilon = 0.2, Br = 3.0, \varphi = 0.15, \beta = 0.01, \gamma = 0.01$.

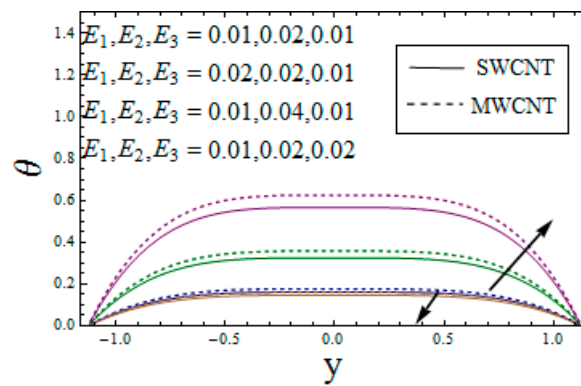


Figure 9. E_1, E_2, E_3 versus θ when $\varphi = 0.15, t = 0.1, x = 0.2, \varepsilon = 0.2, Br = 3.0, Gr = 3.0, \beta = 0.01, \gamma = 0.01$.

To know the influence of pertinent parameters on the entropy generation, Figures 10–13 are sketched. Figure 10 elucidates the impact of φ on the entropy generation. Observations reveal that by enhancing φ entropy generation shows decrease. The main reason behind this behavior is the decrease in temperature by increasing nanoparticle volume fraction. As entropy is directly affected by temperature, it also decreases. This is larger for the case of MWCNT than SWCNT. Increment in N_s is observed for enhancement in Grashof number (see Figure 11). Temperature is related to average kinetic energy of particles. Therefore temperature enhances for higher values of Gr , hence enhancing entropy generation. By increasing the ratio of Br to Λ , the enhancement in entropy generation is noticed (see Figure 12). The Brinkman group parameter $Br\Lambda^{-1}$ shows significance of viscous effects and directly related with the viscosity of nanofluid (see Equation (19)). The Brinkman group parameter and square of velocity is directly related. Therefore, increase in the value of parameter causes velocity to accelerate and as a result entropy increases. The same result is shown by Abbas et al. [38]. The wall properties impact on N_s is seen from Figure 13. It is noticed that with increase in E_1 and E_2 , N_s increases while it decays for the case of E_3 . For the whole discussion, the values for SWCNT is less than the MWCNT.

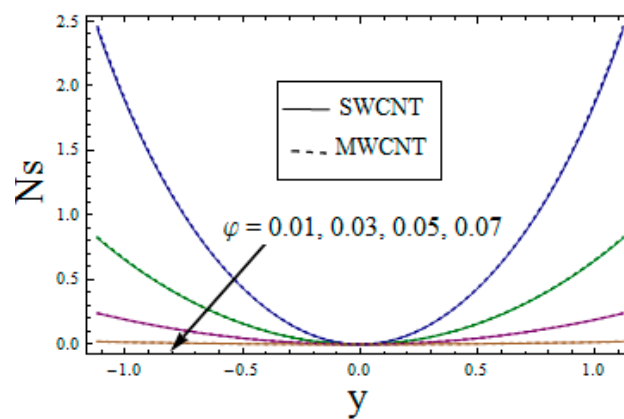


Figure 10. φ versus N_s when $E_1 = 0.02, E_2 = 0.01, E_3 = 0.01, t = 0.1, x = 0.2, \varepsilon = 0.2, Br\Lambda^{-1} = 1.0, Gr = 3.0, \beta = 0.01, \gamma = 0.01$.

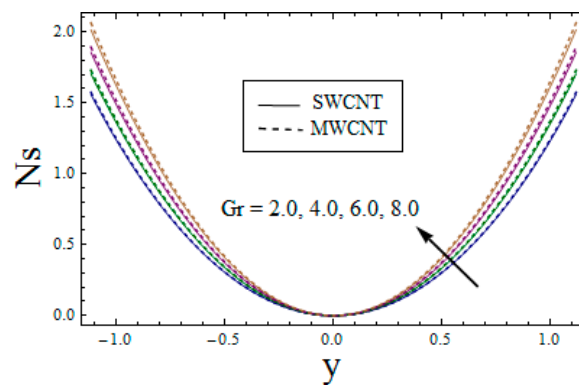


Figure 11. Gr versus Ns when $E_1 = 0.02, E_2 = 0.01, E_3 = 0.01, t = 0.1, x = 0.2, \varepsilon = 0.2, Br\Lambda^{-1} = 1.0, \varphi = 0.15, \beta = 0.01, \gamma = 0.01$.

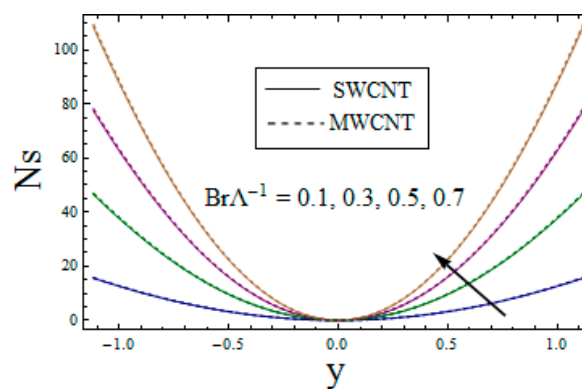


Figure 12. $Br\Lambda^{-1}$ versus Ns when $E_1 = 0.02, E_2 = 0.01, E_3 = 0.01, t = 0.1, x = 0.2, \varepsilon = 0.2, \varphi = 0.15, Gr = 3.0, \beta = 0.01, \gamma = 0.01$.

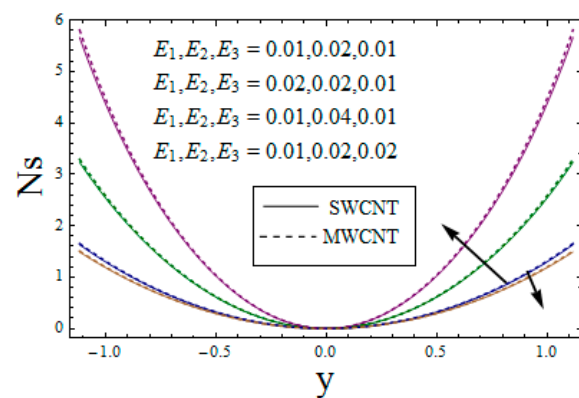


Figure 13. E_1, E_2, E_3 versus Ns when $t = 0.1, x = 0.2, \varepsilon = 0.2, \varphi = 0.15, Br\Lambda^{-1} = 1, Gr = 3.0, \beta = 0.01, \gamma = 0.01$.

For impact of Bejan number, we plotted Figures 14–17. Figure 14 shows the influence of nanoparticle volume fraction on Bejan number. Decrease is noted for Bejan number via enhancing the volume fraction of nanoparticles. Figure 15 depicts the increasing behavior of Grashof number by enhancement in Gr . Via Figure 16, we have seen that by increasing the ratio of Br to Λ Bejan number increases. The result is similar to the one mentioned in [39]. The wall properties impact on Bejan number is seen from Figure 17. There is an enhancement in Bejan number for larger E_1 and E_2 while Bejan number decreases for the case of E_3 . Increase in Bejan number while enhancing pertinent

parameters show that heat transfer irreversibility is high in comparison to the total irreversibility due to heat transfer and fluid friction.

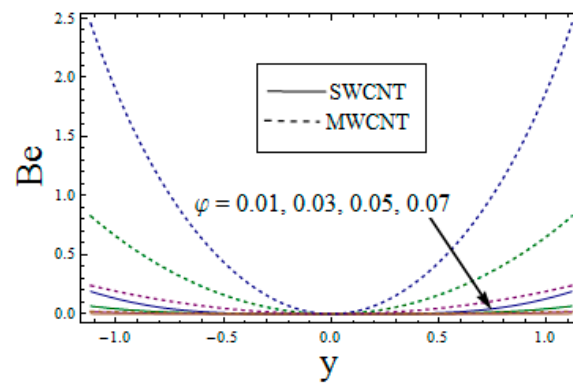


Figure 14. φ versus Be when $E_1 = 0.02, E_2 = 0.01, E_3 = 0.01, t = 0.1, x = 0.2, \varepsilon = 0.2, Br\Lambda^{-1} = 1.0, Gr = 3.0, \beta = 0.01, \gamma = 0.01$.

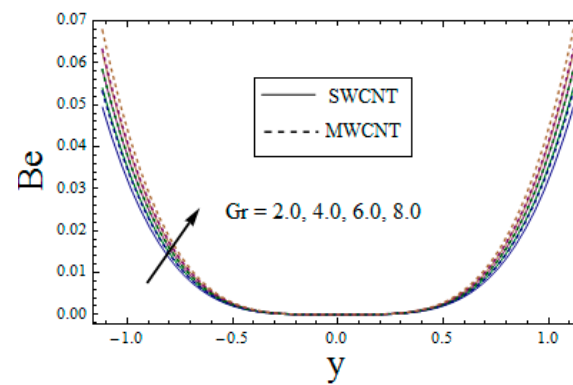


Figure 15. Gr versus Be when $E_1 = 0.02, E_2 = 0.01, E_3 = 0.01, t = 0.1, x = 0.2, \varepsilon = 0.2, Br\Lambda^{-1} = 1.0, \varphi = 0.15, \beta = 0.01, \gamma = 0.01$.

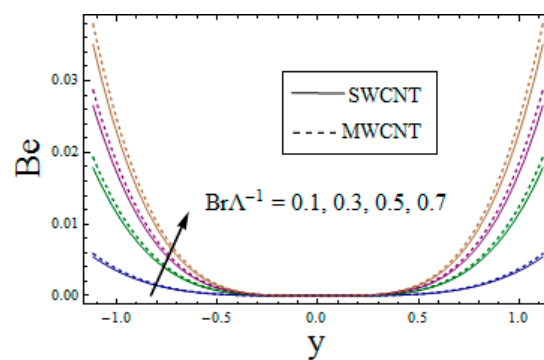


Figure 16. $Br\Lambda^{-1}$ versus Be when $E_1 = 0.02, E_2 = 0.01, E_3 = 0.01, t = 0.1, x = 0.2, \varepsilon = 0.2, Br\Lambda^{-1} = 1.0, \varphi = 0.15, Gr = 3.0, \beta = 0.01, \gamma = 0.01$.

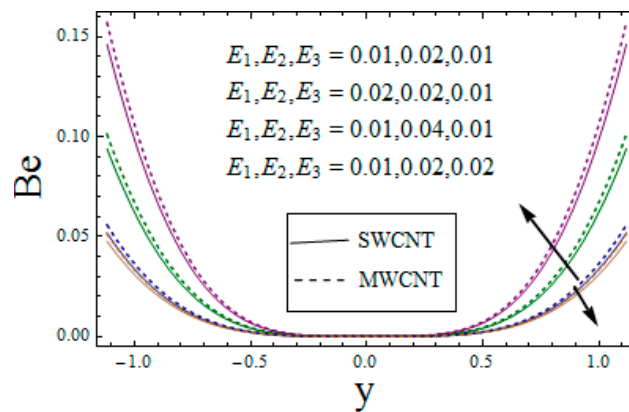


Figure 17. E_1, E_2, E_3 versus Be when $t = 0.1, x = 0.2, \varepsilon = 0.2, Br\Lambda^{-1} = 1.0, \varphi = 0.15, Gr = 3.0, \beta = 0.01, \gamma = 0.01$.

Streamlines are plotted for trapping phenomenon. Figure 18a,b is plotted for trapping regarding SWCNT, whereas Figure 19a,b is sketched for the trapping regarding MWCNT under the impact of slip parameter. Size of trapped bolus increases via slip parameter. Moreover, this increment is larger for SWCNT than MWCNT. Figure 20 addresses the influence of wall parameter on size of trapped bolus for SWCNT. Results show that the size of trapped bolus increases with respect to E_1 and E_2 , whereas it decreases with respect to E_3 . The same result is seen for MWCNT (Figure 21) but increment is more prominent in SWCNT than MWCNT.

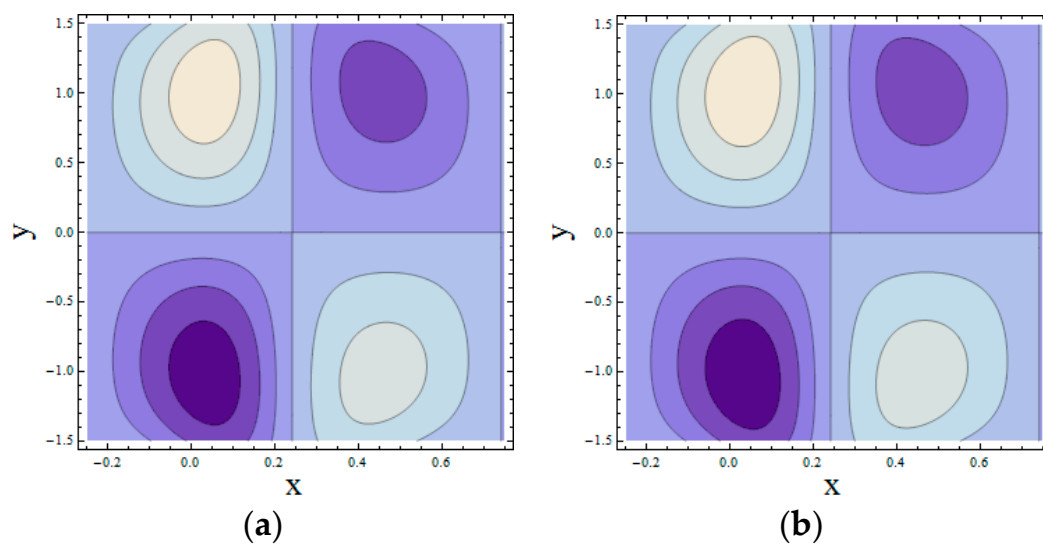


Figure 18. ψ versus β for SWCNT when $E_1 = 0.02, E_2 = 0.01, E_3 = 0.01, t = 0, Br = 3.0, Gr = 3.0, \varepsilon = 0.1, \gamma = 0.01, \varphi = 0.2$: (a) $\beta = 0.01$; and (b) $\beta = 0.03$.

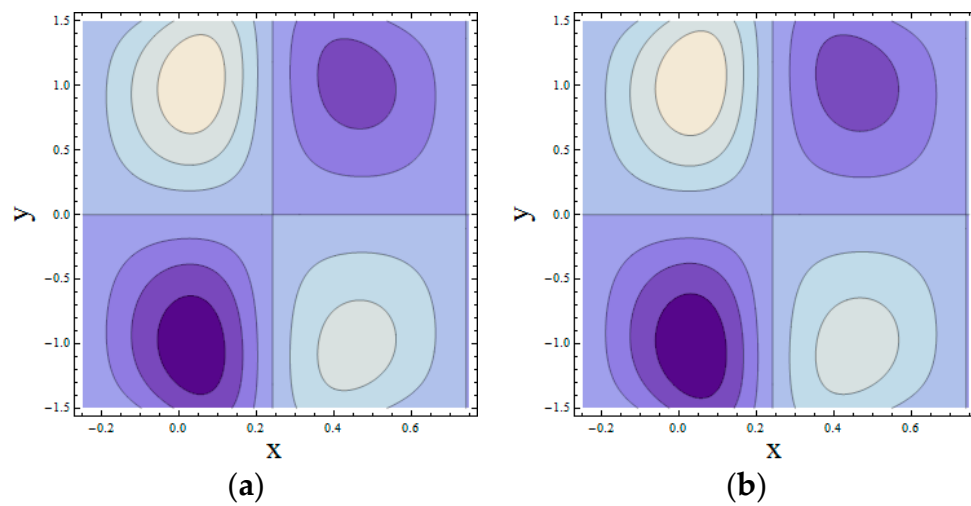


Figure 19. ψ versus β for MWCNT when $E_1 = 0.02, E_2 = 0.01, E_3 = 0.01, t = 0, Br = 3.0, Gr = 3.0, \epsilon = 0.1, \gamma = 0.01, \varphi = 0.2$: (a) $\beta = 0.01$; and (b) $\beta = 0.03$.

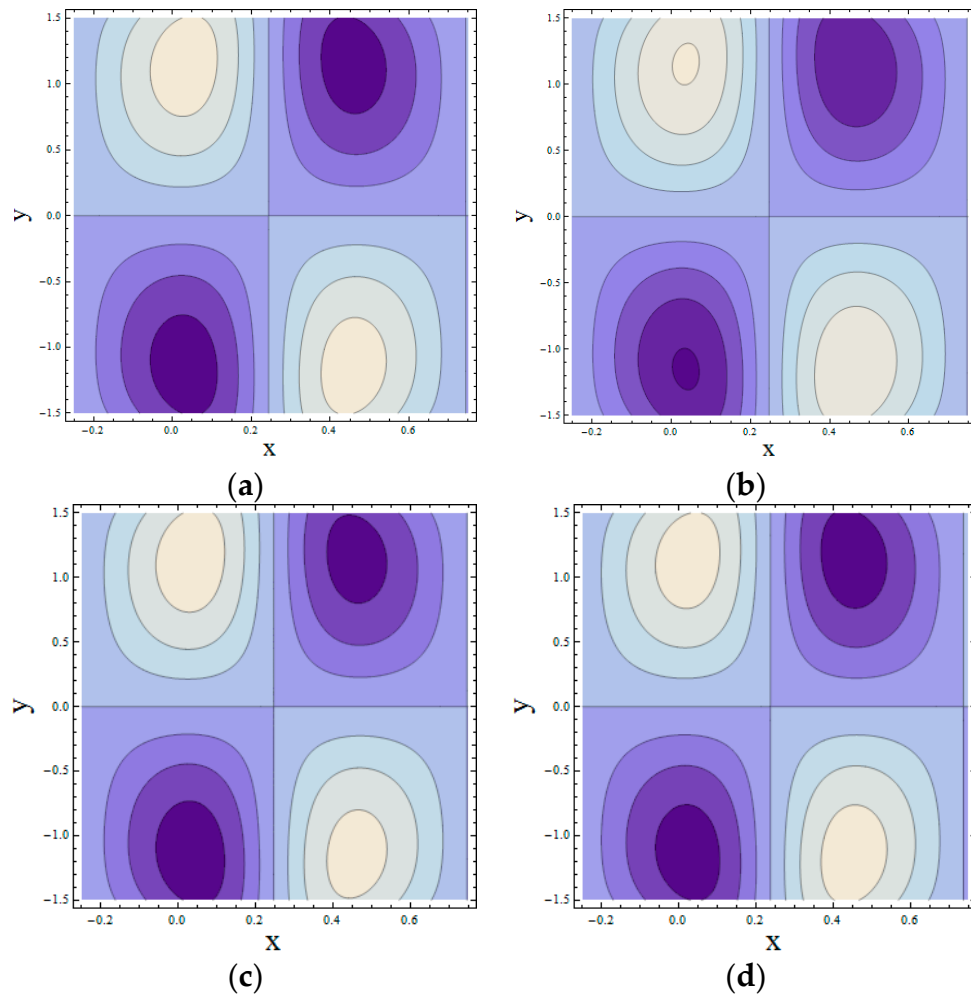


Figure 20. ψ versus E_1, E_2, E_3 for SWCNT when $t = 0, Br = 3.0, Gr = 3.0, \epsilon = 0.1, \beta = 0.01, \gamma = 0.01, \varphi = 0.1$: (a) $E_1 = 0.01, E_2 = 0.03, E_3 = 0.01$; (b) $E_1 = 0.06, E_2 = 0.03, E_3 = 0.01$; (c) $E_1 = 0.01, E_2 = 0.07, E_3 = 0.01$; and (d) $E_1 = 0.01, E_2 = 0.03, E_3 = 0.02$.

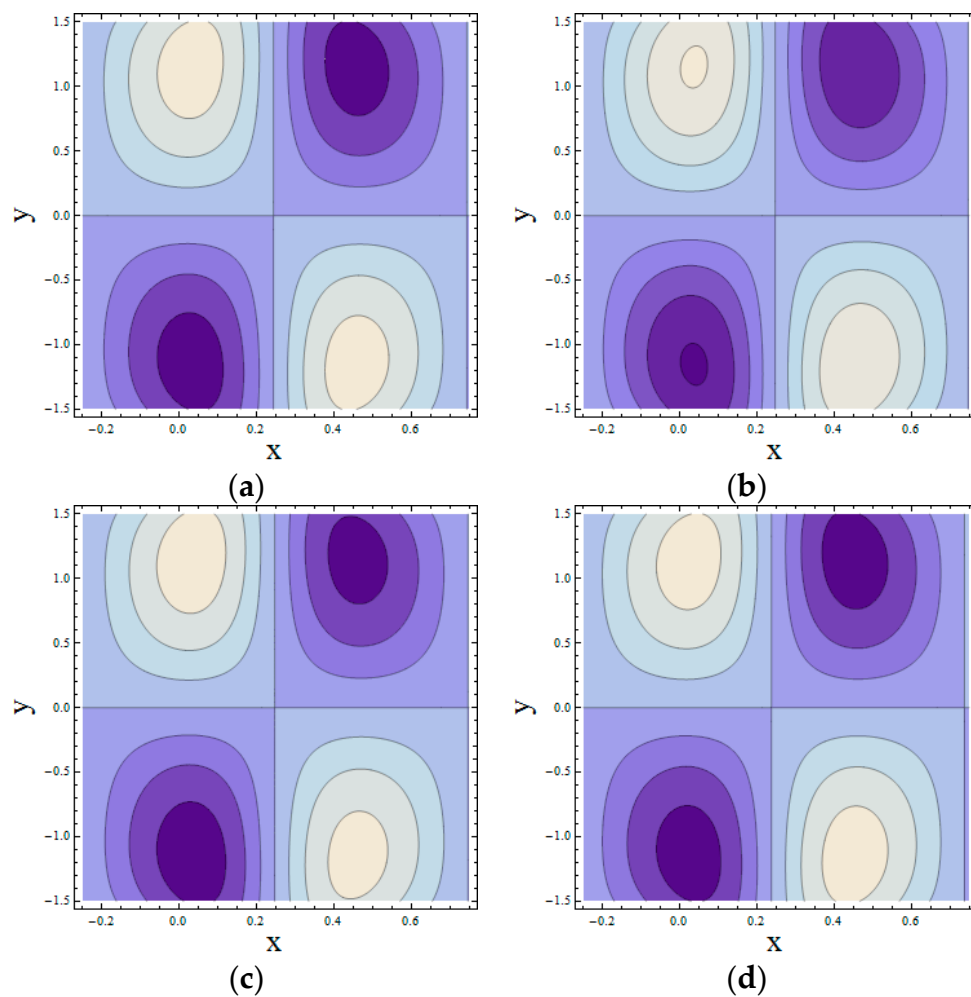


Figure 21. ψ versus E_1, E_2, E_3 for MWCNT when $t = 0, Br = 3.0, Gr = 3.0, \varepsilon = 0.1, \beta = 0.01, \gamma = 0.01, \varphi = 0.1$: (a) $E_1 = 0.01, E_2 = 0.03, E_3 = 0.01$; (b) $E_1 = 0.06, E_2 = 0.03, E_3 = 0.01$; (c) $E_1 = 0.01, E_2 = 0.07, E_3 = 0.01$; and (d) $E_1 = 0.01, E_2 = 0.03, E_3 = 0.02$.

5. Conclusions

The present article addresses the mixed convective peristaltic flow of carbon nanotubes with entropy generation. The main observations are mentioned below:

- Velocity profile is greater in magnitude for MWCNT (multi wall carbon nanotubes) than SWCNT (single wall carbon nanotubes).
- Entropy generation is directly related to Brinkman group parameter $Br\Lambda^{-1}$.
- Inverse relation exists between Bejan number and φ .
- Enhancement in Grashof number Gr and Brinkman group parameter $Br\Lambda^{-1}$ causes an increase in Bejan number.
- Larger values of slip parameters E_1 and E_2 enhance the size of trapped bolus but such size decreases for E_3 .
- Trapped bolus size is larger for SWCNT than MWCNT.

Author Contributions: Tasawar Hayat, Sadaf Nawaz, Ahmed Alsaedi and Maimona Rafiq conceived and designed the mathematical formulation, analyzed the results and wrote this paper. All authors have read and approved the final manuscript.

Conflicts of Interest: The authors declare no conflict of interest.

Nomenclatures

$\eta, -\eta$	right and left walls
t	Time
d	half width of channel
b	wave amplitude
λ	Wavelength
c	wave speed
(x, y)	Cartesian coordinates
(u, v)	velocity components
ρ_{eff}	effective density of nanofluid
μ_{eff}	effective viscosity of nanofluid
$(\rho C)_{eff}$	effective heat capacity of nanofluid
$(\rho\beta)_{eff}$	effective thermal expansion of nanofluid
K_{eff}	effective thermal conductivity
T_0	temperature at walls
p	Pressure
T	fluid temperature
g	Gravity
ϕ	nanoparticle volume fraction
K_f	thermal conductivity of base fluid
K_p	thermal conductivity of nanoparticle
ρ_f, ρ_p	density of fluid and nanoparticle
β_f	fluid thermal expansion coefficient
β_p	nanoparticle thermal expansion coefficient
S	stress tensor
τ	wall elastance parameter
m	mass per unit length
d_1	wall damping parameter
C_f	specific heat of fluid
μ_f	dynamic viscosity of fluid
C_p	specific heat of nanoparticle
β_1	dimensional velocity slip parameter
γ_1	dimensional thermal slip parameter
Pr	Prandtl number
Br	Brinkman number
Re	Reynolds number
δ	wave number
Ec	Eckert number
Gr	Grashof number
ψ	stream function
$E_1, E_2, E_3,$	dimensionless wall parameters
β	dimensionless velocity slip parameter
γ	dimensionless thermal slip parameter
Φ	viscous dissipation
θ_0	reference temperature
Be	Bejan number
φ_m	maximum packing volume fraction
φ_a	effective volume fraction of aggregates
a_a	effective radii of aggregates
a	radius of nanoparticles
D	fractal index

References

1. Choi, S.U.S. Enhancing thermal conductivity of the fluids with nanoparticles. *ASME Fluids Eng. Div.* **1995**, *231*, 99–105.
2. Xue, Q. Model for thermal conductivity of carbon nanotube based composites. *Phys. B Condens. Matter* **2005**, *368*, 302–307. [[CrossRef](#)]
3. Lin, Y.; Zheng, L.; Zhang, X.; Ma, L.; Chen, G. MHD pseudoplastic nanofluid unsteady flow and heat transfer in a finite thin film over stretching surface with internal heat generation. *Int. J. Heat Mass Transf.* **2015**, *84*, 903–911. [[CrossRef](#)]

4. Buongiorno, J. Convective transport in nanofluids. *ASME J. Heat Transf.* **2006**, *128*, 240–250. [[CrossRef](#)]
5. Sheikholeslami, M.; Ganji, D.D. Magnetohydrodynamic flow in a permeable channel filled with nanofluid. *Sci. Iran. B* **2014**, *21*, 203–212.
6. Turkyilmazoglu, M. Nanofluid flow and heat transfer due to a rotating disk. *Comput. Fluids* **2014**, *94*, 139–146. [[CrossRef](#)]
7. Tiwari, R.K.; Das, M.K. Heat transfer augmentation in a two-sided lid-driven differentially heated square cavity utilizing nanofluids. *Int. J. Heat Mass Transf.* **2007**, *50*, 2002–2018. [[CrossRef](#)]
8. Turkyilmazoglu, M. The analytical solution of mixed convection heat transfer and fluid flow of a MHD viscoelastic fluid over a permeable stretching surface. *Int. J. Mech. Sci.* **2013**, *77*, 263–268. [[CrossRef](#)]
9. Sheikholeslami, M.; Ganji, D.D.; Javed, M.Y.; Ellahi, R. Effect of thermal radiation on magnetohydrodynamics nanofluid flow and heat transfer by means of two phase model. *J. Magn. Magn. Mater.* **2015**, *374*, 36–43. [[CrossRef](#)]
10. Khan, J.A.; Mustafa, M.; Hayat, T.; Alsaedi, A. Three-dimensional flow of nanofluid over a nonlinearly stretching sheet: An application to solar energy. *Int. J. Heat Mass Transf.* **2015**, *86*, 158–164. [[CrossRef](#)]
11. Akram, S.; Nadeem, S. Consequence of nanofluid on peristaltic transport of a hyperbolic tangent fluid model in the occurrence of apt (tending) magnetic field. *J. Magn. Magn. Mater.* **2014**, *358*, 183–191. [[CrossRef](#)]
12. Ebdid, A. Remark on the homotopy perturbation method for the peristaltic flow of Jeffrey fluid with nanoparticles in an asymmetric channel. *Comput. Math. Appl.* **2014**, *68*, 77–85. [[CrossRef](#)]
13. Hayat, T.; Farooq, M.; Alsaedi, A. Stagnation point flow of carbon nanotubes over stretching cylinder with slip conditions. *Open Phys.* **2015**, *13*, 188–197. [[CrossRef](#)]
14. Latham, T.W. Fluid Motion in a Peristaltic Pump. Master's Thesis, MIT, Cambridge, MA, USA, 1966.
15. Shapiro, A.H. Pumping and retrograde diffusion in peristaltic waves. In Proceedings of the Workshop in Ureteral Reflux in Children, Washington, DC, USA, 11–12 November 1967; Volume 1, pp. 109–126.
16. Weinberg, S.L. Theoretical and Experimental Treatment of Peristaltic Pumping and Its Relation to Ureteral Function. Ph.D. Thesis, MIT, Cambridge, MA, USA, 1970.
17. Srinivas, S.; Kothandapani, M. Peristaltic transport in an asymmetric channel with heat transfer—A note. *Int. Commun. Heat Mass Transf.* **2008**, *35*, 514–522. [[CrossRef](#)]
18. Asghar, S.; Hussain, Q.; Hayat, T. Peristaltic motion of reactive viscous fluid with temperature dependent viscosity. *Math. Comput. Appl.* **2013**, *18*, 198–220.
19. Mekheimer, K.S.; Elmaboud, Y.A.; Abdellateef, A.I. Particulate suspension flow induced by sinusoidal peristaltic waves through eccentric cylinders: Thread annular. *Int. J. Biomath.* **2013**, *6*, 1350026. [[CrossRef](#)]
20. Hayat, T.; Rafiq, M.; Ahmad, B. Combined effects of rotation and thermal radiation on peristaltic transport of Jeffrey fluid. *Int. J. Biomath.* **2015**, *8*, 1550061. [[CrossRef](#)]
21. Elmaboud, Y.A.; Mekheimer, K.S. Non-linear peristaltic transport of a second-order fluid through a porous medium. *Appl. Math. Model.* **2011**, *35*, 2695–2710. [[CrossRef](#)]
22. Ramesh, K. Influence of heat and mass transfer on peristaltic flow of a couple stress fluid through porous medium in the presence of inclined magnetic field in an inclined asymmetric channel. *J. Mol. Liq.* **2016**, *219*, 256–271. [[CrossRef](#)]
23. Abd-Alla, A.M.; Abo-Dahab, S.M.; Kilicman, A. Peristaltic flow of a Jeffrey fluid under the effect of radially varying magnetic field in a tube with an endoscope. *J. Magn. Magn. Mater.* **2015**, *348*, 79–86. [[CrossRef](#)]
24. Sinha, A.; Shit, G.C.; Ranjit, N.K. Peristaltic transport of MHD flow and heat transfer in an asymmetric channel: Effects of variable viscosity, velocity slip and temperature jump. *Alex. Eng. J.* **2015**, *54*, 691–704. [[CrossRef](#)]
25. Muthuraj, R.; Nirmala, K.; Srinivas, S. Influences of chemical reaction and wall properties on MHD peristaltic transport of a Dusty fluid with Heat and Mass transfer. *Alex. Eng. J.* **2016**, *55*, 597–611. [[CrossRef](#)]
26. Hameed, M.; Khan, A.A.; Ellahi, R.; Raza, M. Study of magnetic and heat transfer on the peristaltic transport of a fractional second grade fluid in a vertical tube. *Eng. Sci. Technol. Int. J.* **2015**, *18*, 496–502. [[CrossRef](#)]
27. Ellahi, R.; Hussain, F. Simultaneous effects of MHD and partial slip on peristaltic flow of Jeffrey fluid in a rectangular duct. *J. Magn. Magn. Mater.* **2015**, *393*, 284–292. [[CrossRef](#)]
28. Abbasi, F.M.; Hayat, T.; Ahmad, B.; Chen, G.Q. Peristaltic motion of non-Newtonian nanofluid in an asymmetric channel. *Z. Naturforsch.* **2014**, *69*, 451–461. [[CrossRef](#)]
29. Abbasi, F.M.; Hayat, T.; Ahmad, B. Impact of magnetic field on mixed convective peristaltic flow of water based nanofluids with Joule heating. *Z. Naturforsch.* **2015**, *70*, 125–132. [[CrossRef](#)]

30. Abbasi, F.M.; Hayat, T.; Ahmad, B. Peristalsis of silver-water nanofluid in the presence of Hall and Ohmic heating effects: Applications in drug delivery. *J. Mol. Liq.* **2015**, *207*, 248–255. [[CrossRef](#)]
31. Shehzad, S.A.; Abbasi, F.M.; Hayat, T.; Alsaadi, F. MHD mixed convective peristaltic motion of nanofluid with Joule heating and thermophoresis effects. *PLoS ONE* **2014**, *9*, e111417. [[CrossRef](#)] [[PubMed](#)]
32. Hayat, T.; Abbasi, F.M.; Al-Yami, M.; Monaqueel, S. Slip and Joule heating effects in mixed convection peristaltic transport of nanofluid with Soret and Dufour effects. *J. Mol. Liq.* **2014**, *194*, 93–99. [[CrossRef](#)]
33. Hayat, T.; Nawaz, S.; Alsaadi, F.; Rafiq, M.; Mustafa, M. A model for an application to biomedical engineering through nanoparticles. *Int. J. Heat Mass Transf.* **2016**, *101*, 112–120. [[CrossRef](#)]
34. Hayat, T.; Nawaz, S.; Alsaadi, A.; Rafiq, M. Mixed convective peristaltic flow of water based nanofluids with Joule heating and convective boundary conditions. *PLoS ONE* **2016**, *11*, e0153537. [[CrossRef](#)] [[PubMed](#)]
35. Gad, N.S. Effect of Hall current on interaction of pulsatile and peristaltic induced flows of a particle-fluid suspension. *Appl. Math. Comput.* **2011**, *217*, 4313–4320. [[CrossRef](#)]
36. Sheikholeslami, M.; Ganji, D.D. Entropy generation of nanofluid in presence of magnetic field using Lattice Boltzmann Method. *Physics A* **2015**, *417*, 273–286. [[CrossRef](#)]
37. Akbar, N.S.; Raza, M.; Ellahi, R. Peristaltic flow with thermal conductivity of H₂O + Cu nanofluid and entropy generation. *Results Phys.* **2015**, *5*, 115–124. [[CrossRef](#)]
38. Abbas, M.A.; Bai, Y.; Rashidi, M.M.; Bhatti, M.M. Analysis of entropy generation in the flow of peristaltic nanofluids in channels with compliant walls. *Entropy* **2016**, *18*, 90. [[CrossRef](#)]
39. Akbar, N.S.; Khan, Z.H. Entropy generation analysis for the peristaltic flow of Cu-water nanofluid with magnetic field in a lopsided channel. *J. Appl. Fluid Mech.* **2016**, *9*, 205–213.
40. Akbar, N.S. Entropy generation analysis for a CNT suspension nanofluid in plumb duct with peristalsis. *Entropy* **2015**, *17*, 1411–1424. [[CrossRef](#)]
41. Halefadl, S.; Estelle, P.; Aladag, B.; Doner, N.; Mare, T. Viscosity of carbon nanotubes water based nanofluids: Influence of concentration and temperature. *Int. J. Therm. Sci.* **2013**, *71*, 111–117. [[CrossRef](#)]
42. Jung, H.M.; Um, S. Thermo-electrical properties of composite semiconductor thin films composed of nanocrystalline grapheme-vanadium oxides. *J. Nanosci. Nanotechnol.* **2014**, *14*, 9051–9059. [[CrossRef](#)] [[PubMed](#)]
43. Kim, D.J.; Nam, S.Y. Characterization of sulfonated silica nanocomposite electrolyte membranes for fuel cell. *J. Nanosci. Nanotechnol.* **2014**, *14*, 8961–8963. [[CrossRef](#)] [[PubMed](#)]



© 2016 by the authors; licensee MDPI, Basel, Switzerland. This article is an open access article distributed under the terms and conditions of the Creative Commons Attribution (CC-BY) license (<http://creativecommons.org/licenses/by/4.0/>).